

# NimbleD: Enhancing Self-supervised Monocular Depth Estimation with Pseudo-labels and Large-scale Video Pre-training

Albert Luginov  and Muhammad Shahzad 

University of Reading  
a.luginov@pgr.reading.ac.uk  
m.shahzad2@reading.ac.uk

**Abstract.** We introduce NimbleD, an efficient self-supervised monocular depth estimation learning framework that incorporates supervision from pseudo-labels generated by a large vision model. This framework does not require camera intrinsics, enabling large-scale pre-training on publicly available videos. Our straightforward yet effective learning strategy significantly enhances the performance of fast and lightweight models without introducing any overhead, allowing them to achieve performance comparable to state-of-the-art self-supervised monocular depth estimation models. This advancement is particularly beneficial for virtual and augmented reality applications requiring low latency inference. The source code, model weights, and acknowledgments are available at <https://github.com/xapaxca/nimbleD>.

**Keywords:** Monocular Depth Estimation · Self-supervised Learning · Knowledge Distillation

## 1 Introduction

Monocular depth estimation (MDE) is the task of predicting the distances to objects relative to the camera from a single image input. Low latency depth estimation is crucial for metaverse applications as it ensures real-time, accurate spatial awareness and immersive interactions with virtual and real-world objects, enhancing user experience and comfort. Recent advancements in vision transformers (ViT) [6], large vision models [25], and generative models [28] have significantly advanced MDE [1, 2, 14, 18, 24, 30, 35, 40]. The two main training paradigms commonly used for MDE are supervised and self-supervised learning (SSL). Supervised MDE relies on ground truth depth labels obtained from LiDAR or RGB-D cameras, whereas SSL MDE leverages geometric constraints from monocular videos or stereo setups. On one hand, SSL MDE models [44] trained exclusively on monocular videos represent the most accessible approach since they require only monocular videos for training, without the need for a stereo setup and ground truth depth, potentially allowing for training on large-scale unlabeled data [34]. On the other hand, the recent supervised models employing large-scale training [40] or generative methods [18] have demonstrated

superior zero-shot depth estimation capabilities. However, these models are often relatively slow at inference, limiting their use in metaverse applications where low latency is crucial. Another challenge is the feasibility of training these models for companies or individuals with limited resources. In this work, we address these challenges by introducing NimbleD, a straightforward yet effective SSL MDE learning framework enhanced by pseudo-labels generated by a large vision model and large-scale video pre-training. This framework noticeably boosts the depth estimation quality of fast and lightweight models without introducing any overhead, enabling them to achieve the performance of larger state-of-the-art SSL MDE methods.

Our contributions are summarized as follows:

- Develop an effective training strategy that utilizes both self-supervision from monocular videos and pseudo-supervision from disparities generated by a large vision model.
- Introduce a concise loss function that combines SSL and PSL losses.
- Incorporate large-scale video pre-training from publicly available videos without any complex data preparation.
- Boost the depth estimation performance of fast and lightweight models to a level comparable to state-of-the-art SSL MDE methods.

## 2 Related Work

Recent advancements in zero-shot MDE have yielded significant progress. MiDaS [2, 27] has effectively addressed training challenges on diverse datasets by implementing a scale- and shift-invariant loss, ensuring compatibility with various ground truth forms. Similarly, ZoeDepth’s [1] innovative two-stage framework integrates relative and metric depth estimation, utilizing large-scale pre-training alongside domain-specific fine-tuning, augmented by a novel bin adjustment mechanism for scale-aware predictions. ZeroDepth’s [14] introduction of input-level geometric embeddings and a variational latent representation has facilitated scale-aware depth estimation across diverse domains, leveraging extensive labeled and synthetic datasets. UniDepth [24] introduces a module that learns camera parameters and uses a pseudo-spherical representation to separate the camera and depth components, demonstrating superior metric depth estimation. KBR’s [34] self-supervised learning approach capitalizes on a vast dataset derived from YouTube, covering a wide array of environments without necessitating camera intrinsics. Marigold [18] employs diffusion-based image generators alongside a fine-tuned Stable Diffusion [28] model with synthetic data, whereas DMD’s [30] diffusion-based method incorporates field-of-view augmentation and log-scale depth representation, further refined through fine-tuning on a varied dataset mix. DepthAnything [40] stands out by proposing a large-scale training regimen for DPT [26], utilizing an extensive dataset coupled with knowledge distillation, semantic supervision, and CutMix [41] data augmentation, showcasing a wide-ranging and innovative approach within the field.

Self-supervised MDE trained exclusively on monocular videos was first introduced by Zhou *et al.* [44]. Monodepth2 [13] further advanced the field by addressing challenges associated with occluded objects and objects moving at the same speed as the camera. Following these foundational works, significant progress has been made. This includes recent works focusing on depth network architecture enhancements [15, 38] and incorporation of additional supervisory signals [23, 43].

There are studies aimed at developing lightweight MDE models that employ mobile architectures. LiteMono [42] utilizes a custom hybrid CNN-Transformer encoder, while SwiftDepth [22] uses SwiftFormer [31] as an encoder accompanied by a custom two-stage decoder. Both models exhibit competitive depth estimation quality with fewer parameters and faster inference speeds, making them ideal for augmented and virtual reality applications.

Various works explore knowledge distillation techniques. Wang *et al.* [37] propose a method that distills knowledge from the teacher model at both the feature and output levels, utilizing silog [8], gradient matching [27], and pairwise distillation [19] losses. TIE-KD [3] focuses on output-level knowledge distillation, employing Kullback-Leibler divergence and SSIM [39] for the loss function. MViTDepth [9] combines self-supervised learning with knowledge distillation, using the logarithm of the L1 difference at the output level. MAL [5] is a multi-frame MDE method that leverages additional supervision from an instance segmentation model to identify moving objects and performs knowledge distillation at the output level using the L1 difference.

In this work, we address the progress in zero-shot MDE by leveraging a modern large vision model to generate pseudo-labels, introducing a straightforward yet efficient loss function, and applying large-scale video pre-training. Our approach ensures that lightweight self-supervised MDE methods match the depth estimation quality of larger state-of-the-art models, making them suitable for real-time applications in the metaverse.

### 3 Method

In this section, we introduce NimbleD learning framework. First, the problem statement of self-supervised MDE enhanced by pseudo-labels is introduced. Next, the combined SLL and PSL loss function is detailed. Finally, the large-scale video pre-training without camera intrinsics is described.

#### 3.1 Self-supervised Monocular Depth Estimation Enhanced by Pseudo-labels

Self-supervised MDE is generally formulated as an image reconstruction problem. Depth estimation serves as a building block of the entire training framework, which is then used independently during inference. The framework consists of a depth network that predicts disparities  $d_t$  from a target frame  $I_t$  and a pose network that predicts the relative camera pose  $T$  between the target frame  $I_t$

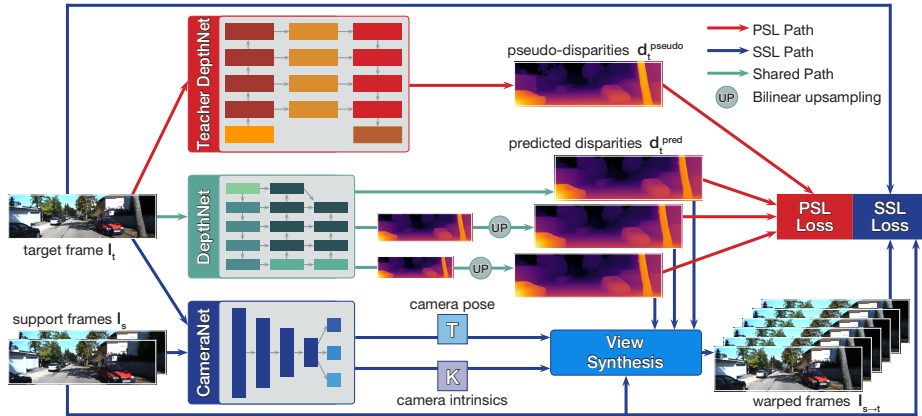


**Fig. 1:** Overview of the proposed NimbleD learning framework. The framework comprises a depth network that outputs multi-scale disparity predictions ( $d_t^{\text{pred}}$ ), a camera network that outputs the relative camera pose ( $T$ ) and camera intrinsic parameters ( $K$ ), and a teacher depth network that generates pseudo-disparities ( $d_t^{\text{pseudo}}$ ). The ultimate objective of the method is to minimize the loss between the predicted and pseudo-disparities (*PSL Loss*) and to minimize the image reconstruction loss (*SSL Loss*).

and support frames  $I_s$ , where  $s \in \{t-1, t+1\}$  indicates the frames temporally adjacent to the target frame. Given depth map  $D_t$ , which is the inverse of disparities ( $1/d_t$ ), camera pose  $T$ , and camera intrinsics  $K$  that must usually be known beforehand, the target frame is reconstructed from support frames  $I_s$  as follows:

$$I_{s \rightarrow t} = I_s \langle \text{proj}(D_t, T, K) \rangle, \quad (1)$$

where  $I_{s \rightarrow t}$  represents the reconstructed target image,  $\text{proj}()$  denotes the projection of depth onto the support frames  $I_s$  coordinates, and  $\langle \rangle$  signifies a differentiable sampling operator [17].

Following [34], the pose network is assigned to learn camera intrinsics  $K$ . The only modification introduced to the network involves adding two additional output heads to the decoder: the first outputs the focal lengths, and the second outputs the principal point coordinates, which together construct the intrinsics matrix  $K$ . Since it predicts all camera parameters (both extrinsic and intrinsic), we refer to it as the camera network.

Supervised MDE is generally formulated as the minimization of error between predicted and ground truth depth maps. Considering situations where ground truth information is unavailable, we employ a large vision model to generate pseudo-labels and minimize the error between predictions and these pseudo-labels. This pseudo-supervisory signal enhances our self-supervised image reconstruction problem and can be seen as offline knowledge distillation at the output level.

The proposed NimbleD learning framework is depicted in Fig. 1.

### 3.2 Combined Self-supervised and Pseudo-supervised Loss Function

We propose a simple yet effective combination of losses widely used in self-supervised and supervised MDE. Our total loss is a weighted average of SSL and PSL losses, averaged across the upsampled multi-scale outputs of the depth network. It is defined as:

$$L_{\text{total}} = \frac{1}{n} \sum_{i=1}^n (\lambda L_{\text{SSL}}^i + (1 - \lambda) L_{\text{PSL}}^i), \quad (2)$$

where  $\lambda$  is the loss weighting parameter, and  $n$  denotes the number of output scales.

The main building block of the SSL loss is photometric error, defined as:

$$\text{pe}(I_t, I_{s \rightarrow t}) = \frac{\alpha}{2} (1 - \text{SSIM}(I_t, I_{s \rightarrow t})) + (1 - \alpha) \|I_t - I_{s \rightarrow t}\|_1, \quad (3)$$

where SSIM denotes the Structural Similarity Index Measure [39], and  $\alpha$  is set to 0.85.

The SSL loss is the per-pixel minimum reprojection loss with auto-masking [13], defined as:

$$L_{\text{SSL}} = \text{mean} \left( \mu \min_{s \in \{t-1, t+1\}} \text{pe}(I_t, I_{s \rightarrow t}) \right), \quad (4)$$

where  $\mu$  represents the auto-masking function, given by:

$$\mu = \left[ \min_{s \in \{t-1, t+1\}} \text{pe}(I_t, I_{s \rightarrow t}) < \min_{s \in \{t-1, t+1\}} \text{pe}(I_t, I_s) \right], \quad (5)$$

where  $[\cdot]$  is the indicator function, which equals 1 if the enclosed condition is true and 0 otherwise.

The PSL loss is defined as a scale-and-shift invariant loss [27], calculated in the disparity space:

$$L_{\text{PSL}} = \text{mean} \left( \left| \hat{d}_{\text{pred}} - \hat{d}_{\text{pseudo}} \right| \right), \quad (6)$$

where  $\hat{d}_{\text{pred}}$  and  $\hat{d}_{\text{pseudo}}$  are the scaled and shifted predicted and pseudo-disparities, respectively. These are defined as follows:

$$\hat{d} = \frac{d - \text{median}(d)}{\text{mean}(|d - \text{median}(d)|)}. \quad (7)$$

It is important to note that widely used smoothness regularization loss [12] was not employed due to its negligible impact on the results [33], see ablation studies. This decision is made to save training time during the large-scale video pre-training.

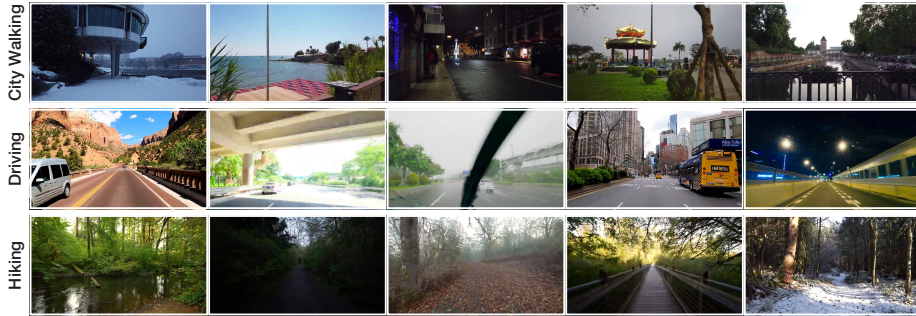


**Fig. 2:** The dataset for large-scale video pre-training is curated from publicly available videos. It consists of three equally represented classes - city walking, driving, and hiking - offering a diverse range of outdoor environments.

**Table 1:** Summary of the dataset for large-scale video pre-training. The dataset includes three balanced classes, each characterized by a diverse set of filming conditions, totaling more than 1.1 million frame triplets.

Class	#Videos	Duration (h)	#Frames	#Triplets	
				Large set	Small set
City walking	35	23.1	383,199	363,973	19,156
Driving	35	23.1	400,617	380,518	20,029
Hiking	35	23.1	392,446	372,758	19,618
Total	105	69.7	1,176,262	1,117,249	58,803

### 3.3 Large-Scale Video Pre-training

NimbleD’s camera network, which predicts camera intrinsics, enables the use of any video with moving cameras and objects. Therefore, we select YouTube videos with a CC-BY license for large-scale pre-training.

We categorize the selected videos into three classes to ensure a diverse range of outdoor environments: driving, hiking, and city walking. The driving class comprises videos from the USA and China, featuring a variety of driving conditions. The hiking videos, filmed in the woods of national parks across the USA, provide natural, uneven terrain. The city walking videos, covering urban areas in Europe and Asia, offer a mix of architectural styles and pedestrian scenarios. Each class includes 35 videos, with each totaling approximately 23 hours, resulting in a 70-hour dataset. Unlike SlowTV [34], our dataset ensures a more balanced composition by maintaining a similar number of frames in each class, as summarized in Tab. 1.

The videos are downloaded at a resolution of  $480 \times 854$  to manage space efficiently, and frames are extracted at a rate of 5 fps to balance motion detail with dataset size. The dataset encompasses a variety of lighting conditions, weather scenarios, and filming challenges. For example, some driving videos are filmed

with a camera installed inside a vehicle, capturing reflections and raindrops on the windshield, as well as the movement of the wipers. City walking videos may display abrupt camera movements, resulting in reduced overlap between frames. Hiking footage often suffers from motion blur and defocusing issues.

Despite these challenges, we decide against pre-processing the videos or the extracted frames, aiming to present the data in its most authentic form, embracing the imperfections and variability inherent in real-world footage. This approach ensures that the dataset reflects genuine outdoor conditions, making it a valuable resource for developing and testing self-supervised MDE models. Some samples from the dataset are presented in Fig. 2.

Our dataset ultimately comprises 1.1M overlapping triplets. Additionally, we create a smaller set of 59K triplets for debugging.

## 4 Experiments

In this section, we first briefly introduce the datasets used and the evaluation metrics. Then, we describe the training implementation details, followed by the evaluation results. Finally, an extensive ablation study is performed to explore various components of our framework.

### 4.1 Datasets

In addition to the aforementioned selected publicly available videos, we utilize KITTI [11], NYUv2 [32], and Make3D [29].

For training on KITTI, we use Eigen-Zhou split [44], which consists of 39,810 automotive outdoor frame triplets. For evaluation on KITTI, we employ Eigen split [7], which includes 697 frames with LiDAR-based ground truth depth, adhering to the standard evaluation protocol. This protocol includes Garg crop [10], 80-meter distance cap, and input resolution of  $192 \times 640$ . Additionally, for comparison with the teacher model, we use Eigen-Benchmark split [36], which comprises 652 frames with improved LiDAR-based ground truth depth, and in this context, we forego cropping.

For zero-shot generalization, we turn to NYUv2 and Make3D, which are not seen by the teacher depth network. NYUv2 encompasses 654 indoor frames with ground truth depth sourced from an RGB-D camera. This evaluation leverages Eigen crop [8], 10-meter distance cap, and input resolution of  $288 \times 384$ . Make3D consists of 134 outdoor frames with laser-based ground truth depth. We use 70-meter distance cap, center crop, and input resolution of  $192 \times 640$ .

Across these evaluation scenarios, we consistently employ a set of standard evaluation metrics [8]. For NYUv2 and Make3D, we use AbsRel, SqRel, RMS, and  $\text{RMS}_{\log}$ . For evaluation on KITTI, we additionally use  $\delta_1 < 1.25$ ,  $\delta_2 < 1.25^2$ , and  $\delta_3 < 1.25^3$ .

**Table 2:** Training details. Training consists of two stages: pre-training on publicly available YouTube videos and fine-tuning on KITTI [11]. *LR* stands for learning rate.

	Pre-training	Fine-tuning
Dataset	YouTube videos	KITTI [11]
Color Jitter	✓	✓
Horizontal flip	✓	✓
Aspect augmentation	✓	
Batch size	16	16
#Epochs	6	20
Training time (h)	32	5
Optimizer	AdamW [21]	AdamW [21]
Weight decay	$10^{-3}$	$10^{-3}$
Initial LR	$10^{-4}$	$10^{-4}$
LR scheduler	Cosine [20]	Step
Adjusted LR	$10^{-5}$	$10^{-5}$
Adjustment epoch	4	10
Loss weighting $\lambda$	0.9	0.9 (0.95 for last 5 ep.)

## 4.2 Implementation Details

For the teacher depth network, we utilize DepthAnything [40], chosen for its high-quality results. Specifically, its ability to generate a large volume of pseudo-labels with limited computational resources stands out, contrasting with diffusion-based models [18]. Notably, DepthAnything is not trained on the KITTI [11], NYUv2 [32], or Make3D [29] datasets. We observe its optimal performance at a resolution of  $518 \times 518$ , rather than at the original input image size. Therefore, we first resize the original images to  $518 \times 518$  and then interpolate the predictions back to the original image size. To maintain the integrity of the pseudo-labels, we store the disparities without normalization and also preserve the maximum value to facilitate information retrieval.

For the depth network, we utilize several baseline methods: Monodepth2 [13], SwiftDepth [22], and LiteMono [42], each with different configurations. Monodepth2 is the standard baseline model for SSL MDE research, while SwiftDepth and LiteMono are fast and lightweight models. The encoders of all depth networks are pre-trained on ImageNet [4]. To ensure that the predicted disparities are consistent with the teacher model, we replace the output activation function from sigmoid to ReLU, thereby eliminating the need for output rescaling to a specific range.

For the camera network, we employ the widely-used PoseNet [13, 44], based on an ImageNet [4] pre-trained ResNet-18 [16] backbone, to ensure compatibility with established methods. We modify the decoder to also output camera intrinsics, in line with KBR [34].

For training, we apply standard data augmentations [13] to the frames fed into the depth network. Additionally, for large-scale video pre-training, we employ aspect ratio augmentations similar to those used in KBR [34], involving

**Table 3:** Results on KITTI [11] Eigen split [7] with median alignment. The input image size is  $192 \times 640$ . *Par* indicates the total number of parameters in millions. The highest scores are highlighted in **bold**, while the second-highest scores underlined.

Method	Venue	Lower is better					Higher is better		
		Par	AbsRel	SqRel	RMS	RMS <sub>log</sub>	$\delta_1$	$\delta_2$	$\delta_3$
DaCCN [15]	ICCV'23	13.0	0.099	<u>0.661</u>	4.316	0.173	0.897	0.967	<u>0.985</u>
GasMono [43]	ICCV'23	27.9	0.098	-	4.303	0.173	0.903	0.968	0.984
FGTO [23]	CVPR'24	27.9	0.096	0.696	4.327	0.174	0.904	0.968	<u>0.985</u>
SQLdepth [38]	AAAI'24	31.1	<b>0.091</b>	0.713	<u>4.204</u>	<u>0.169</u>	<b>0.914</b>	0.968	0.984
MD2-R18 [13]	ICCV'19	14.8	0.115	0.903	4.863	0.193	0.877	0.959	0.981
+ <i>NimbleD (ours)</i>	-	14.8	0.100	0.739	4.440	0.175	0.898	0.967	<u>0.985</u>
MD2-R50 [13]	ICCV'19	34.6	0.110	0.831	4.642	0.187	0.883	0.962	0.982
+ <i>NimbleD (ours)</i>	-	34.6	0.097	0.721	4.377	0.172	0.904	0.968	<u>0.985</u>
SwiftDepth-S [22]	ISMAR'23	3.6	0.110	0.830	4.700	0.187	0.882	0.962	0.982
+ <i>NimbleD (ours)</i>	-	3.6	0.098	0.733	4.401	0.174	0.901	0.968	<u>0.985</u>
SwiftDepth [22]	ISMAR'23	6.4	0.107	0.790	4.643	0.182	0.888	0.963	0.983
+ <i>NimbleD (ours)</i>	-	6.4	0.096	0.697	4.333	0.171	0.905	<u>0.969</u>	<b>0.986</b>
LiteMono-S [42]	CVPR'23	<b>2.5</b>	0.110	0.802	4.671	0.186	0.879	0.961	0.982
+ <i>NimbleD (ours)</i>	-	<b>2.5</b>	0.099	0.709	4.370	0.172	0.898	0.967	<b>0.986</b>
LiteMono [42]	CVPR'23	<u>3.1</u>	0.107	0.765	4.561	0.183	0.886	0.963	0.983
+ <i>NimbleD (ours)</i>	-	<u>3.1</u>	0.096	0.684	4.304	0.171	0.903	<u>0.969</u>	<b>0.986</b>
LiteMono-8M [42]	CVPR'23	8.8	0.101	0.729	4.454	0.178	0.897	0.965	0.983
+ <i>NimbleD (ours)</i>	-	8.8	<u>0.092</u>	<b>0.646</b>	<b>4.194</b>	<b>0.165</b>	<u>0.910</u>	<b>0.970</b>	<b>0.986</b>

center cropping at randomly selected aspect ratios followed by interpolation to sizes that approximate the total pixel counts of a  $192 \times 640$  input size.

Training is conducted on a single NVIDIA GeForce RTX 4090 GPU. All training details are summarized in Tab. 2.

### 4.3 Results

**Evaluation on KITTI.** We evaluate our method on KITTI [11] using Eigen split [7] with median alignment, comparing it with baseline models and leading state-of-the-art single-frame SSL MDE methods, as shown in Tab. 3. First, it is clear that NimbleD significantly enhances the performance of all the baseline models. The method revitalizes Monodepth2-R18 [13], while SwiftDepth [22] and LiteMono [42] perform on par with FGTO [23]. Meanwhile, LiteMono-S and SwiftDepth-S, which offer the best speed and accuracy trade-off on the market, are not far behind DaCCN [15] and GasMono [43]. Moreover, LiteMono-8M demonstrates state-of-the-art performance similar to SQLdepth [38].

We also compared our method to the teacher model, DepthAnything [40], on KITTI [11] Eigen-Benchmark [36] split with improved ground truth using

**Table 4:** Results on KITTI [11] KITTI Eigen-Benchmark [36] splits with improved ground truth against the teacher model using least-squares alignment. The input image size is  $350 \times 350$  and  $518 \times 518$  for DepthAnything [40] and  $192 \times 640$  for methods enhanced by NimbleD. *Par* indicates the total number of parameters in millions. The highest scores are highlighted in **bold**, while the second-highest scores underlined.

Method	Lower is better						Higher is better		
	Par	AbsRel	SqRel	RMS	RMS <sub>log</sub>	$\delta_1$	$\delta_2$	$\delta_3$	
DepthAnything [40] $350 \times 350$	335.3	0.071	0.432	3.504	0.122	0.947	0.989	<u>0.997</u>	
DepthAnything [40] $518 \times 518$	335.3	<b>0.064</b>	<b>0.363</b>	<b>3.239</b>	<u>0.111</u>	<b>0.957</b>	<b>0.991</b>	<u>0.997</u>	
MD2-R18 [13] + <i>NimbleD</i>	14.8	0.073	0.448	3.610	0.122	0.941	0.988	0.996	
MD2-R50 [13] + <i>NimbleD</i>	34.6	0.070	0.438	3.571	0.134	0.945	0.989	<u>0.997</u>	
SwiftDepth-S [22] + <i>NimbleD</i>	3.6	0.072	0.441	3.585	0.120	0.943	0.989	<u>0.997</u>	
SwiftDepth [22] + <i>NimbleD</i>	6.4	0.069	0.408	3.469	0.117	0.946	<u>0.990</u>	<u>0.997</u>	
LiteMono-S [42] + <i>NimbleD</i>	<b>2.5</b>	0.072	0.437	3.584	0.124	0.940	0.988	<u>0.997</u>	
LiteMono [42] + <i>NimbleD</i>	<u>3.1</u>	0.070	0.427	3.537	0.126	0.944	0.989	<u>0.997</u>	
LiteMono-8M [42] + <i>NimbleD</i>	8.8	<u>0.065</u>	<u>0.374</u>	<u>3.338</u>	<b>0.110</b>	<u>0.951</u>	<b>0.991</b>	<b>0.998</b>	

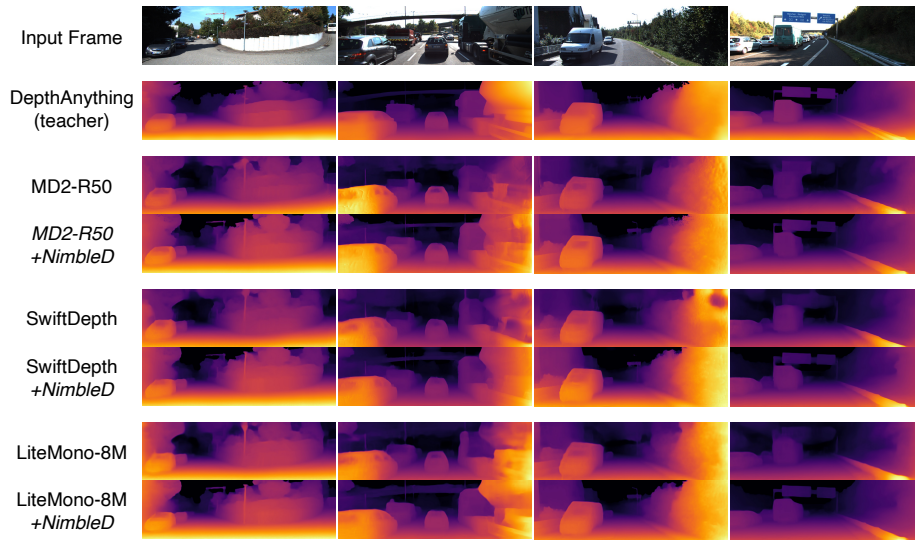


**Fig. 3:** Qualitative results on KITTI [11] Eigen split [7], compared with the teacher model [40] and baseline models [13, 22, 42]. NimbleD observably enhances the depth estimation quality of all baseline models. It identifies distant objects not detected by the teacher model and demonstrates improved handling of sky regions compared to the baseline models.

least squares alignment, which is the standard for evaluating supervised MDE methods, as shown in Tab. 4. Since the teacher model uses a higher input image size, we also included its results with a  $350 \times 350$  input size for a fair comparison,

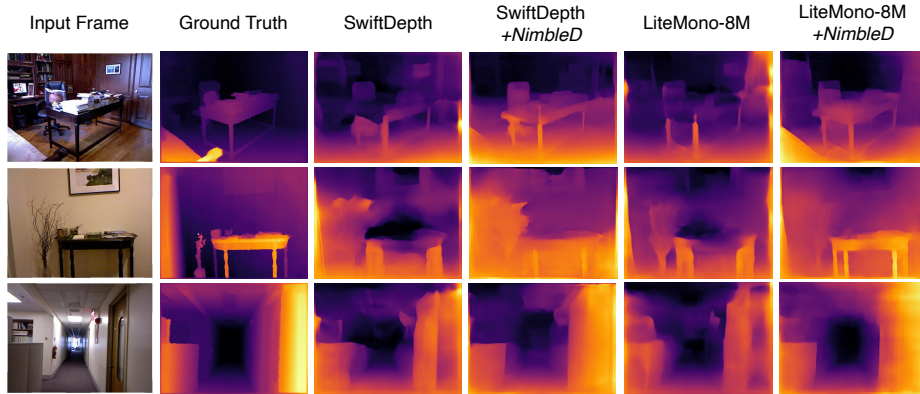


**Fig. 4:** Zero-shot qualitative results on NYUv2 [32], compared to the baseline models [22, 42]. NimbleD noticeably improves the generalization ability of both baseline models.

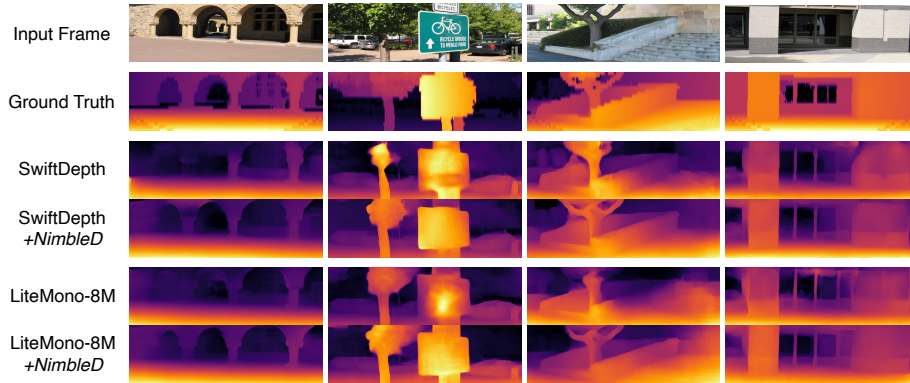


**Fig. 5:** Zero-shot qualitative results on Make3D [29], compared to the baseline models [22, 42]. NimbleD noticeably improves the generalization ability of both baseline models.

which has a pixel count similar to input size of  $192 \times 640$ . Notably, almost all of our models performed similarly to DepthAnything with an input resolution of  $350 \times 350$ , while LiteMono-8M achieved results close to the teacher model’s resolution of  $518 \times 518$ . This demonstrates that NimbleD performs exceptionally well in offline knowledge distillation, considering the number of parameters is reduced by 38 times and the model does not use ground truth data.

The qualitative results compared with DepthAnything, Monodepth2-R50, SwiftDepth, and LiteMono-8M are illustrated in Fig. 3.

**Generalization.** We evaluate the zero-shot generalization of our method on NYUv2 [32] and Make3D [29] by comparing it to baseline models [22, 42]. The

**Table 5:** Zero-shot results on NYUv2 [32] and Make3D [29] against baseline models with median alignment. The input image size is  $288 \times 384$  for NYUv2 and  $192 \times 640$  for Make3D. Lower values are better for all columns.

Method	NYUv2 (indoor) [32]				Make3D (outdoor) [29]			
	AbsRel	SqRel	RMS	RMS <sub>log</sub>	AbsRel	SqRel	RMS	RMS <sub>log</sub>
MD2-R18	0.362	0.665	1.266	0.390	0.322	3.587	7.417	0.163
+ <i>NimbleD</i>	<u>0.237</u>	0.279	0.802	0.281	0.287	3.782	7.179	0.146
MD2-R50	0.326	0.556	1.139	0.358	0.322	3.611	7.326	0.160
+ <i>NimbleD</i>	0.236	0.247	0.764	0.278	0.284	3.477	7.053	0.145
SwiftDepth-S	0.317	0.457	1.070	0.357	0.330	3.909	7.547	0.163
+ <i>NimbleD</i>	<u>0.223</u>	0.240	0.759	0.267	0.293	3.834	7.197	0.146
SwiftDepth	0.277	0.386	0.969	0.314	0.312	<b>3.292</b>	7.125	0.158
+ <i>NimbleD</i>	<b>0.204</b>	<b>0.200</b>	<b>0.689</b>	<b>0.244</b>	0.282	3.708	7.100	<u>0.143</u>
LiteMono-S	0.328	0.537	1.161	0.362	0.332	<u>3.372</u>	7.248	0.167
+ <i>NimbleD</i>	0.236	0.259	0.782	0.287	0.300	4.074	7.382	0.149
LiteMono	0.317	0.488	1.095	0.350	0.317	3.410	7.253	0.161
+ <i>NimbleD</i>	0.243	0.310	0.850	0.295	<u>0.278</u>	3.411	<u>6.979</u>	<u>0.143</u>
LiteMono-8M	0.298	0.415	1.026	0.344	0.318	3.451	7.236	0.159
+ <i>NimbleD</i>	<b>0.204</b>	<u>0.206</u>	<u>0.699</u>	<u>0.253</u>	<b>0.271</b>	3.408	<b>6.952</b>	<b>0.140</b>

results are shown in Tab. 5. NimbleD significantly enhances the models’ generalization ability on NYUv2 (indoor), while the improvement is less notable on Make3D (outdoor). Overall, despite major metric improvements, the results remain unsurprisingly subpar since the models are fine-tuned on KITTI [11]. The qualitative comparison with baseline models on NYUv2 is illustrated in Fig. 4, while the comparison on Make3D is depicted in Fig. 5.

#### 4.4 Ablation Study

We conduct extensive experiments on the components of the loss function, the influence of training without known camera intrinsics, and the impact of large-scale pre-training. SwiftDepth [22] is used as a baseline model. The evaluation results on KITTI [11] Eigen split [7] are presented in Tab. 6. Initially, we replace the output activation function from sigmoid to ReLU in our baseline model, resulting in a minor deterioration of the results. Subsequently, we eliminate the widely-used smoothness regularization loss [13], which does not affect the outcomes. Training without camera intrinsics notably worsens the SSL results, and we note the model’s frequent convergence issues during training. We also evaluate the PSL loss calculation with both single-scale and multi-scale disparity predictions, finding no significant difference between them. To maintain consistency with the SSL loss, we opt for the multi-scale approach. Further experimentation

**Table 6:** Ablation study of loss components, camera intrinsics, and pre-training on the KITTI [11] Eigen split [7] with median alignment. Input image size:  $192 \times 640$ . *Base*: baseline method which is SwiftDepth [22]. *SSL*: self-supervised learning. *PSL*: pseudo-supervised learning. *ReLU*: output activation function is ReLU instead of sigmoid. *multi*: multi-scale outputs. *photo*: photometric error. *min*: minimum reconstruction. *auto*: automasking. *sm*: smoothness loss. *K*: camera intrinsics required. *LSVP*: large-scale video pre-training. \* marks increasing loss weighting  $\lambda$  from 0.9 to 0.95 for the last 5 fine-tuning epochs. The highest scores are highlighted in **bold**, and the second-highest scores are underlined.

Loss	ReLU	multi	photo	min	auto	sm	K	LSVP	Lower is better				Higher is better		
									AbsRel	SqRel	RMS	RMS <sub>log</sub>	$\delta_1$	$\delta_2$	$\delta_3$
Base [22]	✓	✓	✓	✓	✓	✓	✓		0.107	0.790	4.643	0.182	0.888	0.963	0.983
SSL	✓	✓	✓	✓	✓	✓	✓		0.108	0.814	4.624	0.185	0.886	0.963	0.982
SSL	✓	✓	✓	✓	✓	✓	✓		0.107	0.808	4.616	0.184	0.888	0.963	0.982
SSL	✓	✓	✓	✓	✓				0.110	0.878	4.742	0.187	0.887	0.962	0.981
PSL	✓								0.108	0.762	4.735	0.180	0.877	0.963	<b>0.986</b>
PSL	✓	✓							0.108	0.764	4.708	0.179	0.878	0.964	<b>0.986</b>
SSL+PSL	✓	✓	✓	✓	✓		✓		0.101	0.718	4.415	0.175	0.895	<u>0.967</u>	<b>0.986</b>
SSL+PSL	✓	✓	✓	✓	✓				0.101	<u>0.711</u>	4.435	<u>0.174</u>	0.894	<u>0.967</u>	<b>0.986</b>
SSL+PSL	✓	✓	✓	✓					0.104	0.770	4.578	0.176	0.890	<u>0.967</u>	<u>0.985</u>
SSL+PSL	✓	✓	✓						0.103	0.731	4.481	0.175	0.890	0.966	<u>0.985</u>
SSL+PSL	✓	✓	✓	✓	✓		✓		<u>0.097</u>	<u>0.711</u>	<u>4.354</u>	<b>0.171</b>	<u>0.903</u>	<b>0.969</b>	<b>0.986</b>
SSL+PSL*	✓	✓	✓	✓	✓		✓		<b>0.096</b>	<b>0.697</b>	<b>4.333</b>	<b>0.171</b>	<b>0.905</b>	<b>0.969</b>	<b>0.986</b>

**Table 7:** Results on KITTI [11] Eigen split [7] with various values for the loss weighting parameter  $\lambda$ . The table presents averaged results from the last 5 epochs trained solely on KITTI for 20 epochs. The input image size is  $192 \times 640$ . The highest scores are highlighted in **bold**, and the second-highest scores are underlined.

$\lambda$	Lower is better				Higher is better		
	AbsRel	SqRel	RMS	RMS <sub>log</sub>	$\delta_1$	$\delta_2$	$\delta_3$
0.1	0.107	0.722	4.656	0.179	0.879	0.964	<b>0.986</b>
0.3	0.106	0.733	4.651	0.179	0.882	0.964	<b>0.986</b>
0.5	0.105	0.719	4.627	0.177	0.882	0.964	<b>0.986</b>
0.7	0.104	0.713	4.531	<u>0.176</u>	0.887	0.966	<b>0.986</b>
0.8	<u>0.102</u>	<u>0.703</u>	4.458	<b>0.175</b>	0.891	<b>0.967</b>	<b>0.986</b>
0.85	0.102	<b>0.702</b>	4.438	<u>0.176</u>	<u>0.892</u>	<b>0.967</b>	<b>0.986</b>
0.9	<b>0.101</b>	0.720	<b>4.437</b>	<b>0.175</b>	<b>0.895</b>	<b>0.967</b>	<b>0.986</b>
0.95	0.103	0.761	4.518	0.178	<b>0.895</b>	<u>0.966</u>	<u>0.985</u>
0.99	0.113	1.013	4.906	0.216	0.883	0.960	0.980

on the combined SSL and PSL loss with known camera intrinsics reveals a significant improvement in results, indicating a synergistic effect of the combination.

Interestingly, the results remain unchanged when training without camera intrinsics, highlighting the supportive role of PSL for not only improving metrics but also for making training robust in contrast to KBR [34]. We then explore the necessity of minimum reconstruction and automasking [13]; however, omitting them leads to a deterioration in performance. Lastly, we apply large-scale pre-training to our model using the selected combined loss on YouTube videos, followed by fine-tuning on KITTI, which significantly enhances the evaluation metrics. Combined SSL and PSL experiments use a loss weighting parameter  $\lambda$  set to 0.9, determined by extensive manual search as shown in Tab. 7. Interestingly, increasing  $\lambda$  to 0.95 for the last 5 fine-tuning epochs slightly improves and stabilizes results.

## 5 Conclusion

In this work, we introduce NimbleD, an efficient MDE learning framework that enhances SSL using pseudo-labels generated by a large vision model. This approach allows for robust training without camera intrinsics and maintains quality, enabling us to leverage large-scale video pre-training. Consequently, NimbleD elevates the depth estimation performance of fast and lightweight models to match state-of-the-art SSL MDE methods without introducing any overhead, which is advantageous for real-time metaverse applications. While some may argue that using pseudo-supervision from larger models is inequitable, we believe that large vision models are a crucial part of the current deep learning landscape and should be fully utilized.

## References

1. Bhat, S.F., Birkl, R., Wofk, D., Wonka, P., Müller, M.: ZoeDepth: Zero-shot transfer by combining relative and metric depth. arXiv preprint arXiv:2302.12288 (2023)
2. Birkl, R., Wofk, D., Müller, M.: MiDaS v3.1 - a model zoo for robust monocular relative depth estimation. arXiv preprint arXiv:2307.14460 (2023)
3. Choi, S., Choi, D., Kim, D.: TIE-KD: Teacher-independent and explainable knowledge distillation for monocular depth estimation. *Image and Vision Computing* (2024)
4. Deng, J., Dong, W., Socher, R., Li, L.J., Li, K., Fei-Fei, L.: ImageNet: A large-scale hierarchical image database. In: *IEEE/CVF Conference on Computer Vision and Pattern Recognition (CVPR)* (2009)
5. Dong, Y.J., Zhang, F.L., Zhang, S.H.: MAL: Motion-aware loss with temporal and distillation hints for self-supervised depth estimation. In: *IEEE International Conference on Robotics and Automation (ICRA)* (2024)
6. Dosovitskiy, A., Beyer, L., Kolesnikov, A., Weissenborn, D., Zhai, X., Unterthiner, T., Dehghani, M., Minderer, M., Heigold, G., Gelly, S., Uszkoreit, J., Houshy, N.: An image is worth 16x16 words: Transformers for image recognition at scale. In: *International Conference on Learning Representations* (2021)
7. Eigen, D., Fergus, R.: Predicting depth, surface normals and semantic labels with a common multi-scale convolutional architecture. In: *Proceedings of the IEEE International Conference on Computer Vision (ICCV)* (2015)

8. Eigen, D., Puhrsch, C., Fergus, R.: Depth map prediction from a single image using a multi-scale deep network. In: *Advances in Neural Information Processing Systems* (2014)
9. Gao, W., Rao, D., Yang, Y., Chen, J.: Edge devices friendly self-supervised monocular depth estimation via knowledge distillation. *IEEE Robotics and Automation Letters* (2023)
10. Garg, R., Bg, V.K., Carneiro, G., Reid, I.: Unsupervised CNN for single view depth estimation: Geometry to the rescue. In: *European Conference on Computer Vision (ECCV)* (2016)
11. Geiger, A., Lenz, P., Stiller, C., Urtasun, R.: Vision meets robotics: The KITTI dataset. *International Journal of Robotics Research (IJRR)* (2013)
12. Godard, C., Mac Aodha, O., Brostow, G.J.: Unsupervised monocular depth estimation with left-right consistency. In: *Proceedings of the IEEE Conference on Computer Vision and Pattern Recognition (CVPR)* (2017)
13. Godard, C., Mac Aodha, O., Firman, M., Brostow, G.J.: Digging into self-supervised monocular depth estimation. In: *Proceedings of the IEEE/CVF International Conference on Computer Vision (ICCV)* (2019)
14. Guizilini, V., Vasiljevic, I., Chen, D., Amruş, R., Gaidon, A.: Towards zero-shot scale-aware monocular depth estimation. In: *Proceedings of the IEEE/CVF International Conference on Computer Vision (ICCV)* (2023)
15. Han, W., Yin, J., Shen, J.: Self-supervised monocular depth estimation by direction-aware cumulative convolution network. In: *Proceedings of the IEEE/CVF International Conference on Computer Vision (ICCV)* (2023)
16. He, K., Zhang, X., Ren, S., Sun, J.: Deep residual learning for image recognition. In: *Proceedings of the IEEE Conference on Computer Vision and Pattern Recognition (CVPR)* (2016)
17. Jaderberg, M., Simonyan, K., Zisserman, A., Kavukcuoglu, K.: Spatial transformer networks. In: *Advances in Neural Information Processing Systems* (2015)
18. Ke, B., Obukhov, A., Huang, S., Metzger, N., Daut, R.C., Schindler, K.: Repurposing diffusion-based image generators for monocular depth estimation. In: *Proceedings of the IEEE/CVF Conference on Computer Vision and Pattern Recognition (CVPR)* (2024)
19. Liu, Y., Chen, K., Liu, C., Qin, Z., Luo, Z., Wang, J.: Structured knowledge distillation for semantic segmentation. In: *Proceedings of the IEEE/CVF Conference on Computer Vision and Pattern Recognition (CVPR)* (2019)
20. Loshchilov, I., Hutter, F.: SGDR: Stochastic gradient descent with warm restarts. In: *International Conference on Learning Representations* (2017)
21. Loshchilov, I., Hutter, F.: Decoupled weight decay regularization. In: *International Conference on Learning Representations* (2019)
22. Luginov, A., Makarov, I.: SwiftDepth: An efficient hybrid CNN-transformer model for self-supervised monocular depth estimation on mobile devices. In: *2023 IEEE International Symposium on Mixed and Augmented Reality Adjunct (ISMAR-Adjunct)* (2023)
23. Moon, J., Bello, J.L.G., Kwon, B., Kim, M.: From-Ground-To-Objects: Coarse-to-fine self-supervised monocular depth estimation of dynamic objects with ground contact prior. In: *Proceedings of the IEEE/CVF Conference on Computer Vision and Pattern Recognition (CVPR)* (2024)
24. Piccinelli, L., Yang, Y.H., Sakaridis, C., Segu, M., Li, S., Van Gool, L., Yu, F.: UniDepth: Universal monocular metric depth estimation. In: *Proceedings of the IEEE/CVF Conference on Computer Vision and Pattern Recognition (CVPR)* (2024)

25. Radford, A., Kim, J.W., Hallacy, C., Ramesh, A., Goh, G., Agarwal, S., Sastry, G., Askell, A., Mishkin, P., Clark, J., Krueger, G., Sutskever, I.: Learning transferable visual models from natural language supervision. In: Proceedings of the 38th International Conference on Machine Learning (2021)
26. Ranftl, R., Bochkovskiy, A., Koltun, V.: Vision transformers for dense prediction. In: Proceedings of the IEEE/CVF International Conference on Computer Vision (ICCV) (2021)
27. Ranftl, R., Lasinger, K., Hafner, D., Schindler, K., Koltun, V.: Towards robust monocular depth estimation: Mixing datasets for zero-shot cross-dataset transfer. *IEEE Transactions on Pattern Analysis and Machine Intelligence* (2022)
28. Rombach, R., Blattmann, A., Lorenz, D., Esser, P., Ommer, B.: High-resolution image synthesis with latent diffusion models. In: Proceedings of the IEEE/CVF Conference on Computer Vision and Pattern Recognition (CVPR) (2022)
29. Saxena, A., Sun, M., Ng, A.Y.: Make3D: Learning 3D scene structure from a single still image. *IEEE Transactions on Pattern Analysis and Machine Intelligence* (2009)
30. Saxena, S., Hur, J., Herrmann, C., Sun, D., Fleet, D.J.: Zero-shot metric depth with a field-of-view conditioned diffusion model. *arXiv preprint arXiv:2312.13252* (2023)
31. Shaker, A., Maaz, M., Rasheed, H., Khan, S., Yang, M.H., Khan, F.S.: SwiftFormer: Efficient additive attention for transformer-based real-time mobile vision applications. In: Proceedings of the IEEE/CVF International Conference on Computer Vision (ICCV) (2023)
32. Silberman, N., Hoiem, D., Kohli, P., Fergus, R.: Indoor segmentation and support inference from RGBD images. In: European Conference on Computer Vision (ECCV) (2012)
33. Spencer, J., Russell, C., Hadfield, S., Bowden, R.: Deconstructing self-supervised monocular reconstruction: The design decisions that matter. *Transactions on Machine Learning Research* (2022)
34. Spencer, J., Russell, C., Hadfield, S., Bowden, R.: Kick Back & Relax: Learning to reconstruct the world by watching SlowTV. In: Proceedings of the IEEE/CVF International Conference on Computer Vision (ICCV) (2023)
35. Spencer, J., Tosi, F., Poggi, M., Arora, R.S., Russell, C., Hadfield, S., Bowden, R., Zhou, G., Li, Z., Rao, Q., Bao, Y., Liu, X., Kim, D., Kim, J., Kim, M., Lavreniuk, M., Li, R., Mao, Q., Wu, J., Zhu, Y., Sun, J., Zhang, Y., Patni, S., Agarwal, A., Arora, C., Sun, P., Jiang, K., Wu, G., Liu, J., Liu, X., Jiang, J., Zhang, X., Wei, J., Wang, F., Tan, Z., Wang, J., Luginov, A., Shahzad, M., Hosseini, S., Trajcevski, A., Elder, J.H.: The third monocular depth estimation challenge. In: Proceedings of the IEEE/CVF Conference on Computer Vision and Pattern Recognition (CVPR) Workshops (2024)
36. Uhrig, J., Schneider, N., Schneider, L., Franke, U., Brox, T., Geiger, A.: Sparsity invariant CNNs. In: 2017 International Conference on 3D Vision (3DV) (2017)
37. Wang, Y., Li, X., Shi, M., Xian, K., Cao, Z.: Knowledge distillation for fast and accurate monocular depth estimation on mobile devices. In: Proceedings of the IEEE/CVF Conference on Computer Vision and Pattern Recognition (CVPR) Workshops (2021)
38. Wang, Y., Liang, Y., Xu, H., Jiao, S., Yu, H.: SQLdepth: Generalizable self-supervised fine-structured monocular depth estimation. *Proceedings of the AAAI Conference on Artificial Intelligence* (2024)
39. Wang, Z., Bovik, A., Sheikh, H., Simoncelli, E.: Image quality assessment: from error visibility to structural similarity. *IEEE Transactions on Image Processing* (2004)

40. Yang, L., Kang, B., Huang, Z., Xu, X., Feng, J., Zhao, H.: Depth Anything: Unleashing the power of large-scale unlabeled data. In: Proceedings of the IEEE/CVF Conference on Computer Vision and Pattern Recognition (CVPR) (2024)
41. Yun, S., Han, D., Oh, S.J., Chun, S., Choe, J., Yoo, Y.: CutMix: Regularization strategy to train strong classifiers with localizable features. In: Proceedings of the IEEE/CVF International Conference on Computer Vision (ICCV) (2019)
42. Zhang, N., Nex, F., Vosselman, G., Kerle, N.: Lite-Mono: A lightweight CNN and transformer architecture for self-supervised monocular depth estimation. In: Proceedings of the IEEE/CVF Conference on Computer Vision and Pattern Recognition (CVPR) (2023)
43. Zhao, C., Poggi, M., Tosi, F., Zhou, L., Sun, Q., Tang, Y., Mattoccia, S.: GasMono: Geometry-aided self-supervised monocular depth estimation for indoor scenes. In: Proceedings of the IEEE/CVF International Conference on Computer Vision (ICCV) (2023)
44. Zhou, T., Brown, M., Snavely, N., Lowe, D.G.: Unsupervised learning of depth and ego-motion from video. In: Proceedings of the IEEE Conference on Computer Vision and Pattern Recognition (CVPR) (2017)